model domain. The technique for providing boundary conditions is discussed by F. Giorgi [*J. Climate* **3**, 941 (1990)].
18. Neither the Great Salt Lake nor any of the remnant lakes in the Lahontan basin was included in RegCM for the 0-ka simulations because at 60-km resolution the lakes are smaller than the grid in size.
19. S. W. Hostetler and F. Giorgi, *Water Resour. Res.* **29**, 1685 (1993).
20. These results are consistent with the conclusions of McCoy and Williams (*11*), who, on the basis of modeling the 18-ka size of the Little Cottonwood Canyon Glacier, argued that lake-effect precipitation was a substantial component of the hydrologic budget of the lake.
21. It is customary (*2, 9, 10*) to quantify change in basin hydrologic budgets in terms of annual $P - E$, but because our results are for perpetual January and July conditions and not for a complete annual cycle, we cannot infer how the annual hydrologic budgets of the lakes may have changed to support the lakes at their 18-ka sizes.
22. We thank J. E. Kutzbach and P. Behling for providing us with GCM history tapes, L. V. Benson for discussions about this research, and D. L. Zahnle for careful reviews of the manuscript. Support for this research was provided by the National Research Program, Water Resources Division of the U.S. Geological Survey (S.W.H.) and by NSF grants to the National Center for Atmospheric Research (F.G. and G.T.B.) and the University of Oregon (P.J.B.).

3 September 1993; accepted 2 December 1993

Mortality Rates in a Genetically Heterogeneous Population of *Caenorhabditis elegans*

Anne Brooks, Gordon J. Lithgow, Thomas E. Johnson*

Age-specific mortality rates in isogenic populations of the nematode *Caenorhabditis elegans* increase exponentially throughout life. In genetically heterogeneous populations, age-specific mortality increases exponentially until about 17 days and then remains constant until the last death occurs at about 60 days. This period of constant age-specific mortality results from genetic heterogeneity. Subpopulations differ in mean life-span, but they all exhibit near exponential, albeit different, rates of increase in age-specific mortality. Thus, much of the observed heterogeneity in mortality rates later in life could result from genetic heterogeneity and not from an inherent effect of aging.

Human mortality rates show a profound relation with chronological age in that mortality increases exponentially with chronological age from 25 to 30 years of age onward (*1*). Benjamin Gompertz (1825) was the first to recognize this dependency of mortality rate on chronological age and expressed it mathematically by the equation (*1, 2*)

$$m(t) = Ae^{\alpha t}$$

where $m(t)$ is the mortality rate at time t, A is the mortality rate at reproductive maturity, and α is the Gompertz exponent, which describes the rate of acceleration of age-specific mortality with chronological age. The exact shape of the function describing mortality rates in humans has implications for predictions of demographic trends (*3*).

Age-specific mortality rates also increase exponentially with chronological age in a variety of other mammals (*2, 4*) and invertebrates (*4*). Mortality rate is an exponential function of chronological age in *Caenorhabditis elegans* (*5, 6*), and the rate of increase of mortality is genetically specified in recombinant-inbred (RI) strains (*5, 7*). *Age-1* mutant strains also have lower rates of increase of age-specific mortality than wild-type strains (*6*).

In contrast to these observations, recent studies (*8, 9*) have reported that in two insect species—medflies (*Ceratitis capitata*) and the fruit fly (*Drosophila melanogaster*)—mortality rates are not an exponential function of chronological age. In these studies, age-specific mortality rose exponentially for a short period after the emergence of the adult imago but then remained near a high constant level (about 10% mortality per day), or in some cases actually decreased, through the remainder of life. Both studies examined large populations of individuals (up to 1 million medflies), and both argued that exponential increases in mortality in other species are simply an artifact of small population sizes. The resolution of this argument is important because Gompertzian kinetics have become almost synonymous with "true aging" (*4*) and because evolutionary models of aging assume a positive relation [not necessarily exponential (*10*)] between chronological age and mortality rate (*11*).

We report here that the exponential increase in mortality rate that has been consistently observed in *C. elegans* is not an artifact of small population size. We examined mortality kinetics in *C. elegans* in two ways. First, we assayed survival in 180,000 individuals of a single genotype. To do this, we used a sampling procedure in which a small fraction of the population was analyzed for mortality on each day of life. Second, we analyzed the survival of 1625 hermaphrodites of 79 distinct genotypes that were heterogeneous for mean life-span. These results corroborate our earlier studies, in which mortality rates increased exponentially throughout life in small isogenic populations (*5, 6*). These analyses also suggest that age-specific mortality rates in genetically heterogeneous populations appear biphasic because they are comprised of subpopulations, each with differing mortality kinetics. Once the subpopulations with the faster rate of increase of mortality have expired, the age-specific mortality rate of the overall population will appear to decelerate, or even decrease, because the only individuals

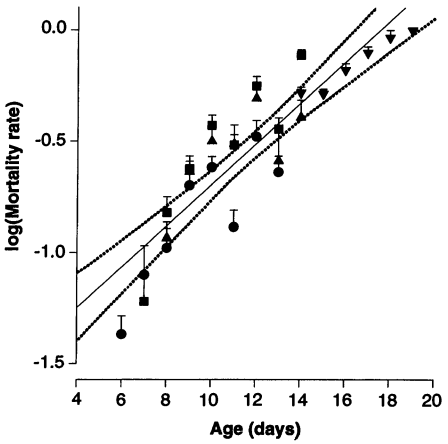

Fig. 1. Age-specific mortality rates (± SEM) of mass cultures of nematodes. A mass culture of TJ1060 [*spe-9(hc88)fer-15(b26)*] was established as described (*12*). We assessed the mean mortality rate by taking eight subpopulations of approximately 25 worms at each age and monitoring daily mortality over a 3-day period in this smaller population, which was maintained under identical conditions as the mass culture, except for nematode density. Symbols: (●) age-specific mortality first day after subculture, (■) age-specific mortality second day after subculture, and (▲) age-specific mortality third day after subculture. Regressions were performed on mortality for each day of subculture; the slopes of these regression lines were not significantly different ($P = 0.38$) nor were the intercepts ($P = 0.25$) by analysis of variance. The mortality rate of the last 824 nematodes (▼) from the starting population of approximately 180,000 is plotted beginning at 15 days of age. The line shown is the least squares regression (±95% confidence interval) of mean daily mortality on age [log (hazard rate) = −1.616 + 0.092 age, $r^2 = 0.789$].

A. Brooks and T. E. Johnson, Institute for Behavioral Genetics and Department of Psychology, University of Colorado, Boulder, CO 80309.
G. J. Lithgow, Institute for Behavioral Genetics, University of Colorado, Boulder, CO 80309.
*To whom correspondence should be addressed.

still living are from subpopulations with lower age-specific mortality rates.

One large isogenic population (TJ1060) was analyzed to see if the mortality rates of this genotype in mass culture were similar to those previously reported (6). Methods for the cultivation of mass cultures of aged C. *elegans* (12) were used to establish age-synchronous cultures of 180,000 nematodes. Mortality was estimated by withdrawing eight samples of 25 nematodes at each time point and assessing daily mortality rates on this subsample over a 3-day period. The increase in mortality rate with chronological age was essentially exponential (Fig. 1) and was independent of the length of time that the subsample had been maintained. Even at older ages, mortality rates continued to increase, although the rate of increase may no longer be exponential. There was little or no evidence of a long period at the end of life where the mortality rate was not a function of chronological age. The last 824 nematodes still alive, representing about 0.4% of the starting population, were also subcultured at 15 days of age and all were followed until dead (Fig. 1). All of these animals were dead by 19 days of age, and the mortality rate of these "oldest old" increased until the end; mortality was 80% (44 dead of 55 total) at 17 days of age and 91% (10 dead of 11 total) at 18 days of age.

Recombinant-inbred strains have been developed by crossing the N2 and Bergerac wild-type strains of C. *elegans*. These RIs display large amounts of genetic variation for length of life (5, 13, 14). As part of a comprehensive examination of quantitative trait loci specifying life-history traits (15), we collected survival data on 79 distinct RIs. Duplicate assessments of survival, each containing 15 hermaphrodites, were collected simultaneously on all 79 RI strains. These replicates were assayed independently and showed a replicability of 0.87 ($P < 0.001$) between means (15). When the survival data from these RIs were assessed, we found kinetics similar to those observed in the medfly (8) and in *Drosophila* (9). The survival curve had a long tail (Fig. 2A), and mortality rates approached 5% daily mortality by 17 days of age and remained at that level for several weeks (Fig. 2B). The same results were observed when either of the two replicate populations of 15 worms was examined separately (Fig. 2, C through F).

To more fully explicate the effect of variation in mortality rate, we ordered the RIs by mean life-span and divided them into contiguous quartiles. We observed quite distinct mean survival times (Table 1) and survival curves (Fig. 3) for each quartile; all are significantly different ($P < 0.001$) from each other. The age-specific mortality rate within each quartile increased almost exponentially with chronological age (Fig. 4). Thus, when genotypes having similar mean life-spans are pooled, the long period of constant mortality rate that was observed in Fig. 2 is all but eliminated and is replaced by kinetics similar to those displayed by mass cultures (Fig. 1) or by smaller populations (5, 6). The differences among quartiles are explained by differences

Table 1. Mean life-spans and variances for each quartile (combined data from replicates 1 and 2).

Quartile	Mean life-span (days)	*n*	Variance (days)	Coefficient of variation (%)
Total	23.01	1625	82.12	39.38
1	14.98	317	19.48	29.46
2	19.69	392	26.80	26.29
3	23.67	443	41.02	27.06
4	30.54	473	99.29	33.63

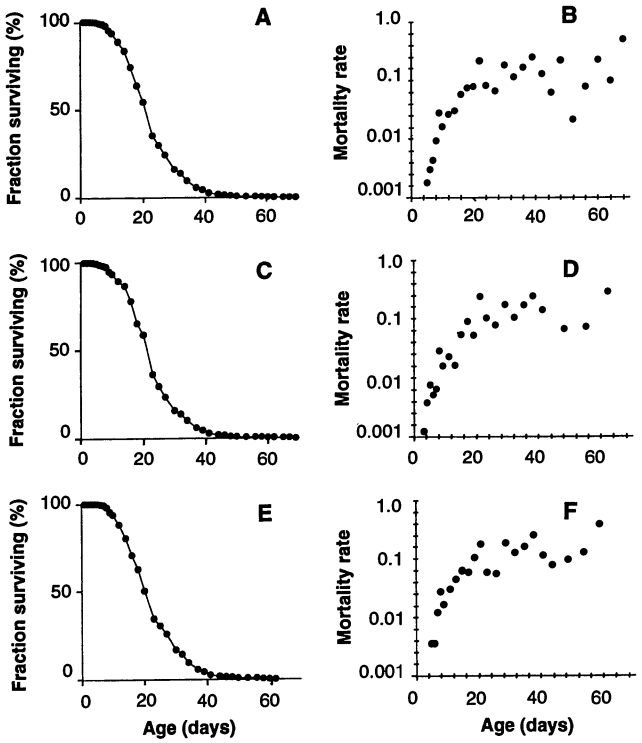

Fig. 2. Survival curve (**A, C,** and **E**) and age-specific mortality rate (**B, D,** and **F**) for the pooled RI strains. We obtained data either by pooling both replicate plates (A and B) of all the RI strains or by examining each replicate separately (Replicate 1, C and D; replicate 2, E and F). Out of a starting population of 2755 nematodes, 1625 died a senescent death and are included in the analysis. Survival analysis was performed, and the age-specific mortality rate was calculated for 1-, 2-, 3-, and 4-day periods throughout life and estimated with the minimum interval in which a nonzero mortality value was observed. All statistical analyses were performed with SPSS/PC 4.0 (16).

Table 2. Weighted, age-specific mortality data for combined RI strains for each quartile.

Quartile	Life-span (days; mean ± SEM)	Weighted Gompertz parameters*		Initial mortality rate (probability of death per day)	Mortality rate doubling time‡ (days)
		A_0 ± SEM†	α ± SEM		
1	14.98 ± 0.25	−2.06 ± 0.04	0.0929 ± 0.002^{A}§	0.0087	3.24
2	19.69 ± 0.26	−2.11 ± 0.06	0.0790 ± 0.003^{B}	0.0078	3.81
3	23.67 ± 0.30	−1.96 ± 0.05	0.0512 ± 0.002^{C}	0.0110	5.88
4	30.54 ± 0.46	−2.01 ± 0.03	0.0334 ± 0.001^{D}	0.0098	9.01

*Mortality rate was weighted by the number of animals dying within any time period, given here as the log of the probability of death per day. †Value is the mortality rate on day 3—typically the first day of reproductive maturity. ‡Calculated from the equation $t_{0.5} = (\log 0.5)/-\alpha$, where $t_{0.5}$ is the mortality rate doubling time and α is the component describing the rate of acceleration of the age-specific mortality rate (2). §Values with different superscripts are significantly different ($P < 0.05$), as calculated with Duncan's multiple range test.

Table 3. Identification of essential parameters by use of a model-comparison approach (DOD is day of death; quart. is quartile) (17).

Source of variance	Variance (%)	F_{inc}	*df**	*P*
Quartile	2		3	
Quart. + DOD	45		1	
Quart. + interaction†	10	106	3,1617	<0.001
Quart. + DOD^2	14	963	1,1616	<0.001
Quart. + interaction‡	10	102	3,1613	<0.001
Quart. + DOD^3	<1	22	1,1612	<0.001

*Degrees of freedom (numerator, denominator) (17). †Interaction of DOD with quartile. ‡Interaction of DOD^2 with quartile.

in α, the Gompertz exponent (Table 2). There is no difference in A_0, initial mortality among the quartiles.

A model-comparison approach (*17*) was used to identify the parameters necessary to accurately model these data. Different models were examined for a significant increase in total variance that was explained by the addition of each new parameter. Within each quartile, the dependence of mortality rate on chronological age is best explained by the addition of a quadratic term that allows for an additional nonlinear component late in life (Table 3). A significant increase in fit is achieved ($P < 0.001$) by addition of this component, which indicates that even within each quartile, the age-specific mortality rate still displays a small nonexponential component. Higher order components offer better fits but explain little additional variance. This nonlinearity may well result from genetic heterogeneity that is still present within each quartile.

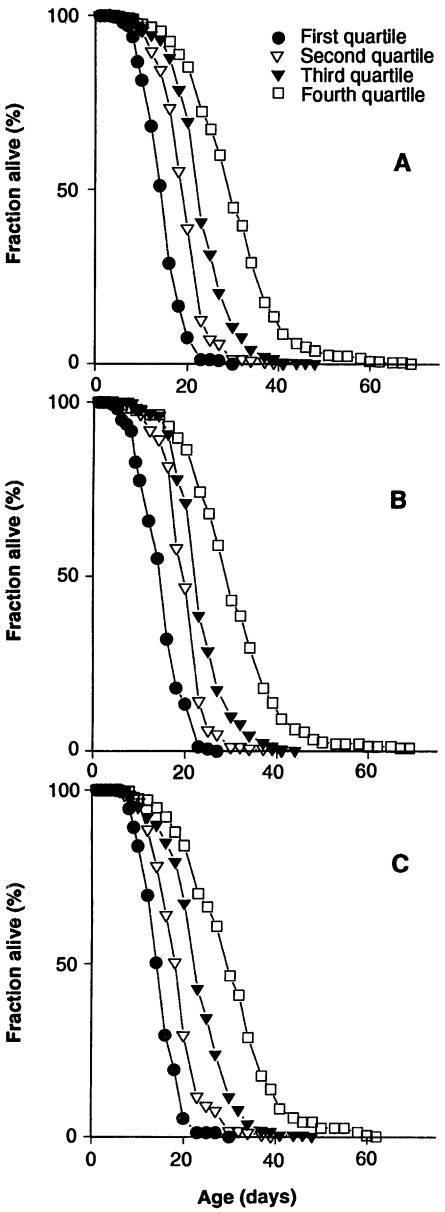

Fig. 3. (**A**) Survival curves for each quartile for the pooled RI strains and for (**B**) replicate 1 and (**C**) replicate 2. We determined quartile placement by calculating the mean life-span of each RI and grouping them into contiguous sets. Descriptive statistics for these data are in Table 1.

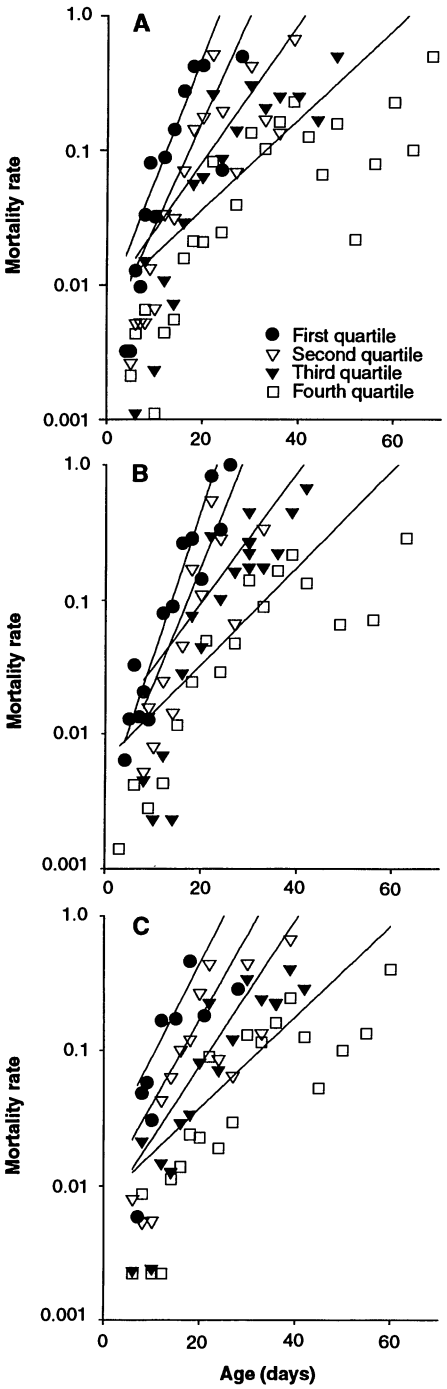

Fig. 4. Age-specific mortality rate and chronological age from the combined data set (**A**), replicate 1 (**B**), or replicate 2 (**C**). Recombinant-inbred strains have been grouped according to quartile as shown in Fig. 3. Survival analysis was performed and the logarithm of the daily hazard rate was regressed on the starting day of the interval, generating the Gompertz parameters that were compared by means of a *t* test. We calculated all mortality rates at intervals of 1 to 7 days, using the minimum interval in which the mortality rate was nonzero.

The combined survival and mortality kinetics of the RI populations closely approximate those previously observed (*8*, *9*). We too observed periods of several weeks when the mortality rate did not increase with chronological age. We ascribe this nonlinearity to genetic effects rather than to innate functions of the populations under study (such as population size), because by establishing subpopulations based on mean life-span we were able to observe age-specific mortality kinetics that were nearly an exponential function of chronological age. Similar kinetics were observed when the population was fractionated into two replicate samples (Fig. 4). Genetic heterogeneity within populations will lead to a deceleration of the age-specific mortality curve as soon as the most at-risk population has expired. The same observations have been made in several other cases and similar suggestions have been put forward (*8*, *18*). Some genetic variation may exist within the medfly populations, and we suggest that those mortality kinetics (*8*) could have resulted from the admixture of a large number of different genotypes into one test population. This interpretation cannot be made of the data on inbred *D. melanogaster* (*9*) because those lines were kept distinct and all flies in each study were of the same genotype. However, even slight contamination with offspring would lead to mortality rate decreases and increases in life expectancy late in life (*12*, *19*).

Even when both environment and genotype have been kept constant, variability in life-span or in other quantitative variables is still observed. In our studies, this variability was a function of average life-span as shown by the constancy of the coefficient of variation (Table 1), which is consistent with the notion that those inbred populations that die late in life are not fundamentally different from those that die early.

The biphasic mortality rate observed in the genetically heterogeneous populations of nematodes results from the genetic heterogeneity of the populations. Genetic heterogeneity could explain similar mortality kinetics in human populations (*1*, *20*) in which, beyond 85 years of age, the mortality rate stops increasing exponentially and becomes constant or actually decreases. Considerations such as these affect the accuracy of demographic predictions of human mortality.

REFERENCES AND NOTES

1. B. Gompertz, *Philos. Trans. R. Soc. London Ser. A* **57**, 289 (1825); L. A. Gavrilov and N. S. Gavrilova, *The Biology of Life Span: A Quantitative Approach*

(Harwood Academic, New York, 1991).
2. G. A. Sacher, in *Handbook of the Biology of Aging*, C. E. Finch and L. Hayflick, Eds. (Van Nostrand Reinhold, New York, 1977), pp. 582–638.
3. C. K. Cassel, M. A. Rudberg, S. J. Olshansky, *Health Aff.* **11**, 87 (1992); J. Fries, *Perspect. Biol. Med.* **31**, 407 (1988); D. B. Brock, J. M. Guralnick, J. A. Brody, in *Handbook of the Biology of Aging*, E. L. Schneider and J. W. Rowe, Eds. (Academic Press, San Diego, CA, ed. 3, 1990), pp. 3–23.
4. C. E. Finch, *Longevity, Senescence, and the Genome* (Univ. of Chicago Press, Chicago, 1990).
5. T. E. Johnson, *Proc. Natl. Acad. Sci. U.S.A.* **84**, 3777 (1987).
6. ———, *Science* **249**, 908 (1990).
7. ———, W. L. Conley, M. L. Keller, *Exp. Gerontol.* **23**, 281 (1988).
8. J. R. Carey, P. Liedo, D. Orozco, J. W. Vaupel, *Science* **258**, 457 (1992).
9. J. W. Curtsinger, H. H. Fukui, D. R. Townsend, J. W. Vaupel, *ibid.*, p. 461.
10. T. B. L. Kirkwood, in *Handbook of the Biology of Aging*, C. E. Finch and E. L. Schneider, Eds. (Van Nostrand Reinhold, New York, ed. 2, 1985), pp. 27–44; C. E. Finch, M. C. Pike, M. Witten, *Science* **249**, 902 (1990).
11. B. Charlesworth, *Evolution in Age-Structured Populations* (Cambridge Univ. Press, Cambridge, 1980); M. R. Rose, *Evolutionary Biology of Aging* (Oxford Univ. Press, Oxford, 1991).
12. T. J. Fabian and T. E. Johnson, *J. Gerontol. Biol. Sci.*, in press.
13. T. E. Johnson and W. B. Wood, *Proc. Natl. Acad. Sci. U.S.A.* **79**, 6603 (1982).
14. A. Brooks and T. E. Johnson, *Heredity* **67**, 19 (1991).
15. ———, unpublished data.
16. M. J. Norussis, *SPSS/PC + 4.0 Base Manual* (Statistical Package for the Social Sciences, Chicago, 1990); ———, *SPSS/PC + Advanced Statistics 4.0* (Statistical Package for the Social Sciences, Chicago, 1990).
17. A model-comparison approach [C. M. Judd and G. H. McClelland, *Data Analysis: A Model Comparison Approach* (Harcourt Brace Jovanovich, San Diego, CA, 1989)] was used to identify the parameters capable of reducing most of the error in predicting these data from a mathematical model. The models were compared as each new parameter was added for a significant increase in total variance that is explained by

$$F_{inc} = \frac{(R^2_{wi} - R^2_{wo})/M}{(1 - R^2_{wi})/df_{res}}$$

where F_{inc} is the incremental F ratio, R^2_{wi} is the multiple R^2 achieved with the new parameter in the equation, R^2_{wo} is the multiple R^2 without the new parameter in the equation, M is the number of new parameters, and df_{res} is the residual degrees of freedom in the final analysis of variance table [B. G. Tabachnick and L. S. Fidell, *Using Multivariate Statistics* (HarperCollins, New York, ed. 2, 1989), p. 157]. The percentage of variance accounted for by each parameter was calculated using Type III (or partial) sums of squares, which are invariant to the order of parameters in the model [*GLM-VARCOMP*, vol. 2 of *SAS/STAT User's Guide* (Statistical Analysis System Institute, Cary, NC, 1990), p. 936].
18. A. Kowald and T. B. L. Kirkwood, *Science* **260**, 1664 (1993).
19. T. J. Fabian and T. E. Johnson, unpublished observations.
20. M. Witten, *Mech. Ageing Dev.* **46**, 175 (1988).
21. We thank T. Reed, T. M. White, and D. Lopez for technical assistance and G. Carey for statistical advice. Supported by grants from NIH (R01-AG08332, R01-AG10248, and K04-AG00369) and by a gift from the Glenn Foundation for Medical Research. Some stocks were supplied by and are available through the Caenorhabditis Genetics Stock Center, which is supported by NIH and the University of Minnesota.

23 September 1993; accepted 8 December 1993

Zinc Finger Phage: Affinity Selection of Fingers with New DNA-Binding Specificities

Edward J. Rebar and Carl O. Pabo

A phage display system was developed and used to select zinc finger proteins with altered DNA-binding specificities. The three zinc fingers of the Zif268 protein were expressed on the surface of filamentous phage, and a library of variants was prepared by randomizing critical amino acids in the first zinc finger. Affinity selections, using DNA sites with base changes in the region recognized by the first finger, yielded Zif268 variants that bound tightly and specifically to the new sites. This phage system provides a tool for the study of protein-DNA interactions and may offer a general method for selecting zinc finger proteins that recognize desired target sites on double-stranded DNA.

Designing and selecting proteins with new DNA-binding specificities can test and extend our understanding of protein-DNA interactions. The zinc finger motif, of the type first discovered in transcription factor IIIA (*1*), offers an attractive framework for these studies. This zinc finger is one of the most common eukaryotic DNA-binding motifs (*2*), and this family of proteins can recognize a diverse set of DNA sequences (*3*). Zinc finger proteins also exhibit a modular organization which suggests that it may be possible to "mix and match" fingers to obtain proteins with novel DNA-binding specificities (*4*, *5*). Crystallographic studies of the Zif268-DNA complex (*4*) and other zinc finger–DNA complexes (*3*, *6*) show that residues at four positions make most of the base contacts, and there has been some discussion about rules or codes that may explain zinc finger–DNA recognition (*7*). However, the recently reported structures of the GLI-DNA complex (*3*) and of the Tramtrack-DNA complex (*6*) show that zinc fingers can dock against the DNA in a variety of slightly different ways. This complexity makes model building and rational design more difficult, but it also reemphasizes the versatility of the zinc finger motif.

Phage display systems have provided powerful selection methods for many studies of peptides and proteins (*8*, *9*). To explore the usefulness of phage display for studying zinc finger–DNA interactions, we first expressed the three Zif268 zinc fingers (*10*) on the surface of filamentous phage (Fig. 1, A and B). The resulting construct—fd-tet.Zif—produced useful titers of "Zif phage" (*11*), and these phage bound specifically to the nine–base pair site recognized by Zif268 (*12*). We then created a library of Zif variants by randomizing the four positions of the first finger that appear most important for making base contacts (*3*, *4*, *6*). These randomized positions include the residue immediately preceding the α helix and include the second, third, and sixth residues of this helix (*13*).

Affinity selection methods were then used to search the library for phage that would recognize altered binding sites. In each round of affinity selection, phage were equilibrated with biotinylated target DNA and then applied to streptavidin-coated microtiter wells. After washing, the retained phage were eluted in high salt buffer, amplified in *Escherichia coli*, and purified to prepare for the next cycle. The target DNA duplexes for these selections contained modified Zif268 binding sites with changes in the region recognized by finger one (*4*), and we refer to each duplex by the sequence of this region (Fig. 1C). Initially, we performed five rounds of selection with each of the target sites (Fig. 1D) (*14*). During these initial selection series, retention efficiencies in the GACC- and GCAC-selected phage pools increased about 100 times, whereas retention efficiencies for the CCTG pool remained low (*15*). We then used these enriched GACC and GCAC pools as a starting point for additional, more stringent selection cycles (Fig. 1D) (*14*). The CCTG pool was not studied further.

Phage pools from critical stages of the GACC and GCAC selections were characterized by sequencing (Fig. 1D), and amino acid preferences were apparent in each pool. For the GACC pool, sequencing after the initial selection series showed that all of the phage (12/12) could be characterized by the consensus sequence (S/D/T)_NR (Table 1). Three additional rounds of selection using high salt washes did not substantially change this consensus (Table 2). For the GCAC selections, sequencing revealed notable changes in the later pools. After the initial selection series, many of the phage belonged to a group characterized by the consensus sequence R_DR (18/22), but there also was a group characterized by the sequence _G(S/T)R (4/22) (Table 1). After additional rounds of selection with high salt washes, a single sequence—RADR—from the first group predominat-

Department of Biology, Massachusetts Institute of Technology, Cambridge, MA 02139.